J. Am. Ceram. Soc., 69 [3] 181–89 (1986)

Implications of Transformation Plasticity in ZrO_2-Containing Ceramics: I, Shear and Dilatation Effects

I-WEI CHEN* and P. E. REYES MOREL

Department of Nuclear Engineering and Department of Materials Science and Engineering, Massachusetts Institute of Technology, Cambridge, Massachusetts 02139

Transformation plasticity in ZrO_2-containing ceramics generally exhibits shear and dilatation effects of comparable magnitude. The coupling between external stresses and crystallographic strains assists the tetragonal-monoclinic transformation, which, via shear localization, gives rise to macroscopic shear and dilatant deformation. Application of a yield criterion based on both shear and dilatation effects correctly correlates deformation data from tension, compression, bending, and indentation, and further delineates a crack-tip process zone comparable to the one observed experimentally. Similar shear and dilatation effects in microcracking due to transformation plasticity are explored. These findings suggest that the strength of the ultimate transformation-toughened structural ceramics should be yield limited and sensitive to the stress state. Strategies for fracture control are recommended.

I. Introduction

SINCE the seminal paper of Garvie, Hannink, and Pascoe was published a decade ago,[1] it has been generally recognized that transformation plasticity induced by the tetragonal (t) to monoclinic (m) transformation is responsible for the remarkable toughening properties of zirconia-containing alloys. Nevertheless, no systematic effort has been made to study transformation plasticity experimentally, and thus far the few theoretical studies of transformation plasticity to crack-tip and other related phenomena have been relatively crude.[2–4] The apparent lack of progress in this important direction is probably due to the relative experimental difficulty of testing ceramic materials in the fully plastic regime, which is further compounded by the complexity of transformation plasticity that is dependent on both hydrostatic and deviatoric stresses. A comprehensive investigation of transformation plasticity thus calls for (a) an improved experimental technique which allows for independent control of the stress states and (b) a modified elastic-plastic analysis which accounts for the pressure effect. This author recently reported the use of the hydraulic compression test for this purpose and demonstrated the pressure sensitivity of the transformation stress and the multiaxiality of the transformation strain.[5] Further investigation along the same line has now fully established the constitutive relation of transformation plasticity in Mg-PSZ.[6] The purpose of the present study is to explore the implications of transformation plasticity in a broader perspective and to demonstrate the effects of its shear and dilatant characteristics on deformation and fracture control in ceramic applications. In the companion paper,[7] a case study of elastic-plastic indentation is made to further demonstrate the implications of transformation plasticity in zirconia-containing ceramics.

The emphasis on the shear and dilatant characteristics of transformation plasticity takes on special importance because of its historical significance in this field, the unique microstructure of partially stabilized zirconia, and the inherent elastic stiffness of ceramic substances. Unlike their metallic counterparts, which exhibit severely sheared, plate- or lathlike martensitic microstrutures at a scale of 10 μm and larger, the transformation-toughened ceramics studied in earlier days contain zirconia particles of 1 μm or smaller. These particles are highly unstable and were retained by virtue of the lack of potent nucleating defects.[8–11] During stress-assisted phase transformation, the growth of the martensitic plate in these ceramics is necessarily restricted to the span of the particle size; yet self-stresses due to the elastic constraint of the particle and the external inert matrix are conducive to autocatalysis of further self-accommodated transformation.[10] These developments give rise to a twinned microstructure in the product phase and appear to have eliminated most of the shear strain overall. Several earlier workers in the field have therefore attributed the transformation toughening entirely to the dilatation from phase transformation and have further suggested that the yield criterion of transformation plasticity be based only on the hydrostatic tension at the crack tip.[2,3] Subsequent refinement of these arguments did consider the shear component of the interaction energy; however, the model assumed a twinned particle whose shape is only slightly biased by the external stress field.[4] As will become clear in subsequent sections, these earlier contentions of the dominance of the dilatation effect are perhaps unrealistic and need to be refined in the future exploration of transformation plasticity in zirconia-containing ceramics.

The interplay between shear and dilatancy in plastic deformation is examined in the first half of the paper. The experimental evidence of shear and dilatation in transformation plasticity is reviewed, with emphasis on the mechanism of shear band formation, and their combined effect is incorporated into the conventional shear-stress-governed yield criterion by the inclusion of pressure hardening. Experimental results from tension, compression, bending, and microindentation are shown to be quantitatively consistent with this criterion. In the second half of the paper, we examine the interplay between shear and dilatation in damage control. The experimental evidence of shear-band-induced microcracking is reviewed, and the enhancement of crack-tip plasticity by the combined shear/dilatation effect is studied. Further experimental evidence consistent with these observations is discussed.

The above considerations lead us to propose a new mechanical approach to the design of structural applications of the ultimate transformation-toughened zirconia ceramics, emphasizing a flaw-tolerant but yield-limited criterion, with special precautions taken against yield sensitivity to the stress state.

II. Hydraulic Compression Experiments

Details of the investigation of transformation plasticity in Mg-PSZ† using hydraulic compression tests will be given elsewhere.[6] All the experimental results, which will be later shown in Figs. 1, 2, 6, 8, 12, and 13 in this paper, were extracted from data and micrographs obtained under conditions nearly identical with those reported in Ref. 6. Therefore, only a brief account is given here to outline experimental procedures. These hydraulic compression tests were performed in a pressure vessel at 30 to 400 MPa. Axial loading was applied to the specimen once a predetermined pressure was reached. The intent of the independent control of pressure and axial compressive stresses was to vary the dilatational and deviatoric driving forces separately and to investigate the interplay between dilatation and shear effects. During these experiments, strains were measured by two pairs of strain gauges mounted on the

Received July 1, 1985; revised copy received November 20, 1985; approved December 5, 1985.

Supported in part by the U.S. Department of Energy under Grant No. DE-FG 02-84ER45154, and support for P. E. Reyes Morel provided by the Government of Chile.

*Member, the American Ceramic Society.

†Nilcra Ceramics, Victoria, Australia.

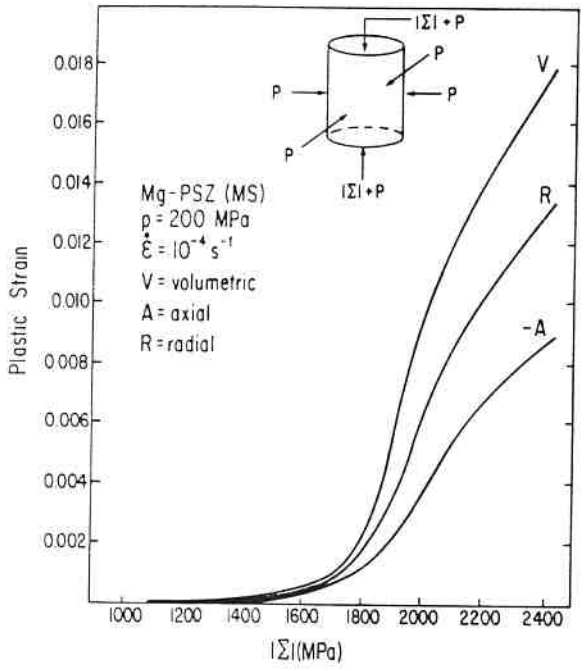

Fig. 1. Plastic strain vs differential stress in hydraulic compression.

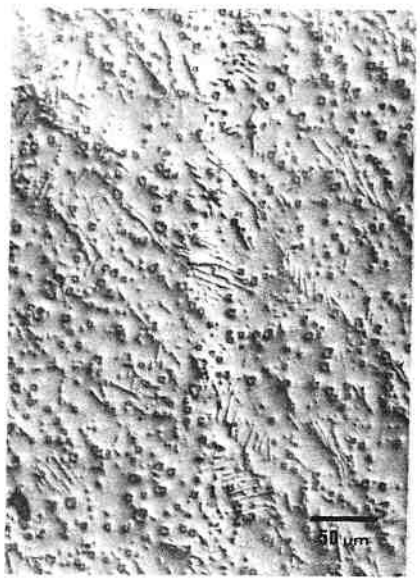

Fig. 2. Micrograph of sample deformed in hydraulic compression, showing shear bands of various orientations. Intersections of bands are seen in several regions. Marker is comparable to grain size.

specimens in the axial and radial directions. Periodic unloading was introduced to monitor the unloading elastic moduli in both directions. The recording of volumetric strains, from the sum of radial and axial strains, allowed us to directly estimate the fraction of transformation of the tetragonal precipitates, which constituted 35% in volume of these materials. The degradation of elastic moduli provided a measure of the microcrack damage accumulated during deformation. Micrographs were taken from internal sections. Shear bands can be revealed, on suitably polished sections, because of the large difference in hardness of the transformed monoclinic phase and the untransformed tetragonal and cubic mixture (see the companion paper for further clarification on this point). Direct evidence of microcracks was also revealed in the nearly fully transformed samples. Crack closure was avoided in this case, because of the lack of significant residual compressive stresses at such advanced stages of transformation in uniformly deformed materials. In general, different polishing conditions are required to enhance the contrast of microcracks and shear bands, respectively.

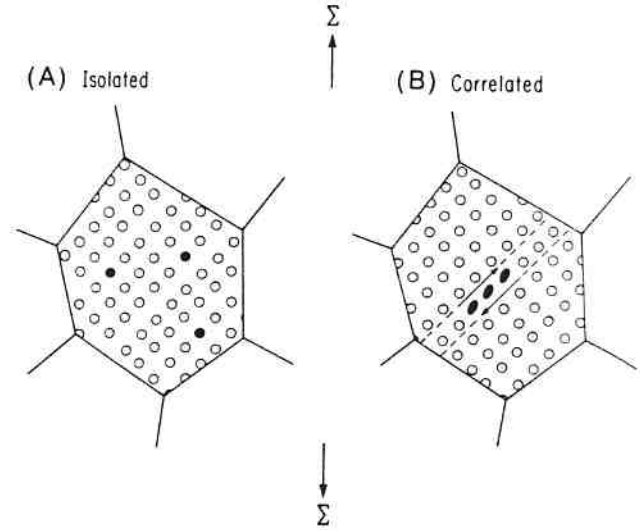

Fig. 3. (*A*) Isolated events producing only volumetric strain and (*B*) correlated events causing autocatalysis and shear bands.

III. Shear and Dilatation Effects on Deformation

To assess the importance of the shear and dilatation effects in transformation plasticity, it is necessary to (a) ascertain the shear and dilatation characteristics of the macroscopic and microscopic strains resulting from transformation and (b) establish the shear and dilatation coupling of the macroscopic and microscopic stresses assisting transformation. We now deal with these aspects separately.

(1) Macroscopic Strains

Under hydraulic compression, in which a uniaxial compressive load is superposed to a triaxial hydraulic pressure onto a cylindrical specimen, Mg-PSZ containing 35% tetragonal inclusions deforms plastically in both the radial and the axial directions, following an initial linear elastic regime. As shown in Fig. 1, the axial strain is compressive and the radial strain is tensile. Thus, both volumetric and deviatoric plastic strains are produced during plastic loading. The ratio of the axial strain, radial strain, and volumetric strain is ≈2:3:4.

It is straightforward to compute the strain deviators, defined as

$$\varepsilon'_{ij} = \varepsilon_{ij} - \delta_{ij}\varepsilon_{ij}/3 \tag{1}$$

where ε_{ij} is the multiaxial plastic strain tensor and δ_{ij} is the Kronecker delta. The second term on the right-hand side is one-third of the volumetric strain ε_v. The equivalent deviatoric plastic strain is defined as

$$\varepsilon_e^2 = \frac{2}{3}\varepsilon'_{ij}\varepsilon'_{ij} \tag{2}$$

where repeated indices are summed over $i, j = 1, 2, 3$. Hence, the ratio of the macroscopic shear to the macroscopic dilatancy is

$$(\varepsilon_e/\varepsilon_v)_{\text{macroscopic}} = -\tfrac{2}{3} \tag{3}$$

where a minus sign is introduced to denote the compressive nature of deformation. Thus, the macroscopic dilatancy triggered by shear has nearly the same magnitude as the macroscopic shear in transformation plasticity.

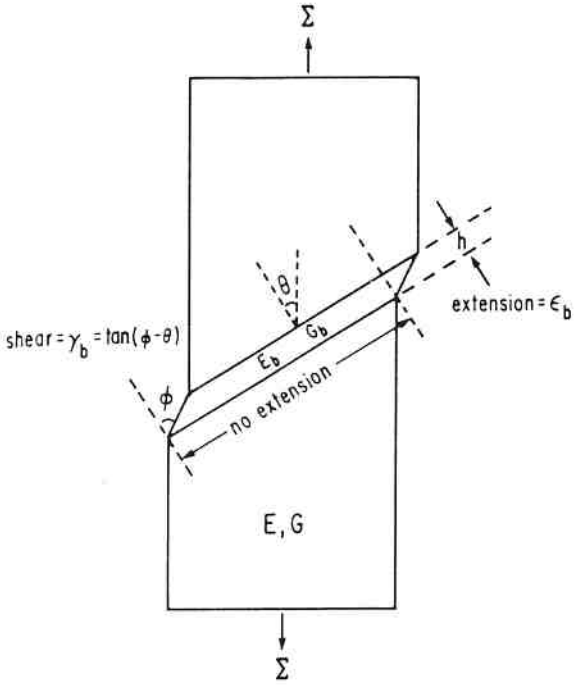

Fig. 4. Configuration of shear band accommodating shear strain by offset and dilatant strain by normal extension. Moduli of band are lower than those of matrix.

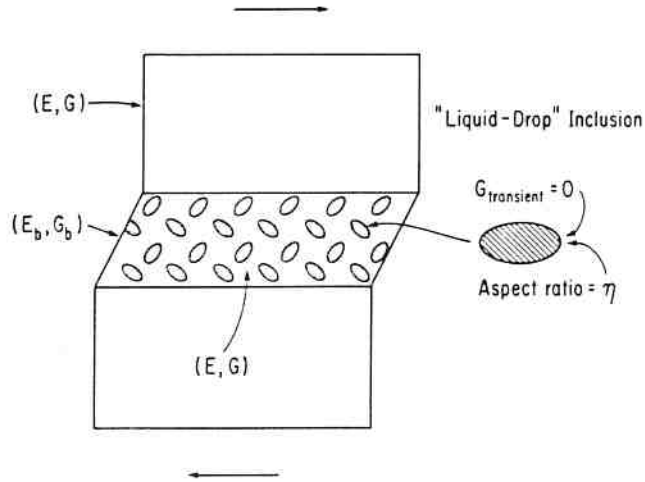

Fig. 5. Schematic illustrating that monoclinic particles in shear band are dynamically soft, behaving like liquid drops.

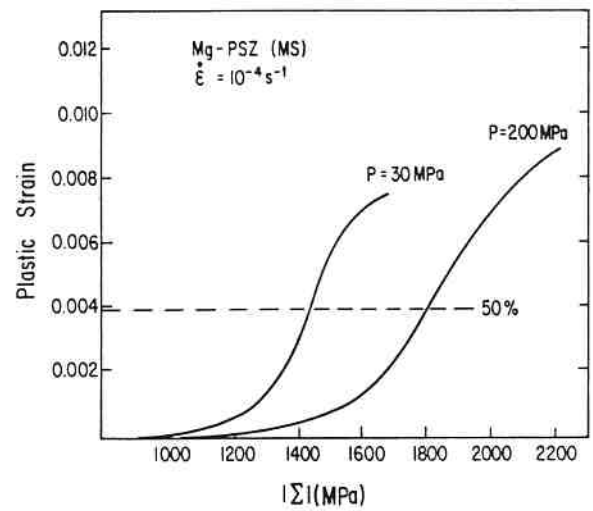

Fig. 6. Plastic axial strain vs differential stress; dashed line represents 50% transformation.

(2) Microscopic Strains

Theoretically, the maximal amount of the shear and dilatation strains available from the *t-m* transformation is given by the unconstrained transformation strains, $s_T = 0.15$ and $\bar{e}_T = 0.04$, where s_T is a simple shear and $\bar{e}_T$ is a volumetric strain. Converting s_T to the equivalent strain, the above transformation strains give

$$(\varepsilon_e/\varepsilon_v)_{\text{microscopic}} = 2.1 \qquad (4)$$

Thus, slightly less than 50% of the microscopic transformation shear strain is eventually manifested in the macroscopic transformation plasticity.

The mechanism by which microscopic strain of transformation is converted to macroscopic strain of plasticity is shear localization, as shown in the micrograph in Fig. 2 for a deformed Mg-PSZ specimen. Since the marker in Fig. 2 is of the order of the grain size in Mg-PSZ, shear bands span the grain but do not cross the grain boundary. The micrograph was taken from an interior section of a deformed cylindrical specimen. Shear bands within the same grain, as revealed by polishing, are apparently parallel to each other, indicating considerable influence on their orientation by the crystallographic and presumably anisotropic elastic properties of the single crystals. Intersections of shear bands can be seen in several regions.

As schematically shown in Fig. 3, shear localization initiated by correlated events of particle transformation is necessary for the manifestation of any macroscopic deviatoric strain. Otherwise, if only transformation of isolated tetragonal particles in a cubic matrix is involved, the considerable elastic stiffness of the inert matrix must force the transformed particle to assume a nearly self-similar shape, even at a considerable external bias of $|\Sigma|/E \approx 10^{-2}$, where $|\Sigma|$ is the applied axial stress and E is Young's modulus, in the hydraulic compression experiment. If this were the case, the net deviatoric strain would have been negligible compared to the volumetric strain.[4] On the other hand, if correlated events eventually trigger shear localization,[5,6] then the shear strain can be partially retained by the shear offset of the band, while the dilatation can still be entirely retained by the normal displacement across the band as shown in Fig. 4. The actual amount of shear retention thus depends on the effective moduli of the shear band. More detailed computation[5,6] based on the composite theory indicates that the ratio of Eq. (3) is explicable if all the inclusions behave as dynamically liquid drops during shear localization (Fig. 5). Since the monoclinic phase twins easily and has an anomalously low yield stress,[7] the above microscopic picture of strain localization appears reasonable.

It seems reasonable to conclude that shear-band formation is the mechanism which converts microscopic transformation strains to macroscopic plastic strains, both of which contain a shear and a dilatation component. In this sense, shear bands in transformation plasticity are functionally equivalent to slip bands in dislocation plasticity, their main difference residing not in the shear characteristics common to both mechanisms but rather in the accompanying dilatant characteristics unique to the shear-band mechanism in (dilatant) transformation plasticity.

(3) Macroscopic Stresses

The macroscopic stress dependence of transformation plasticity also involves both shear and dilatation components. This is because (a) a uniaxial stress causes plastic deformation, indicating its shear coupling, and (b) a superposed hydraulic pressure shifts the axial stress-strain curve to a higher axial stress level, indicating its dilatation coupling. This is illustrated in Fig. 6 for Mg-PSZ tested under hydraulic compression conditions. Considerable strain hard-

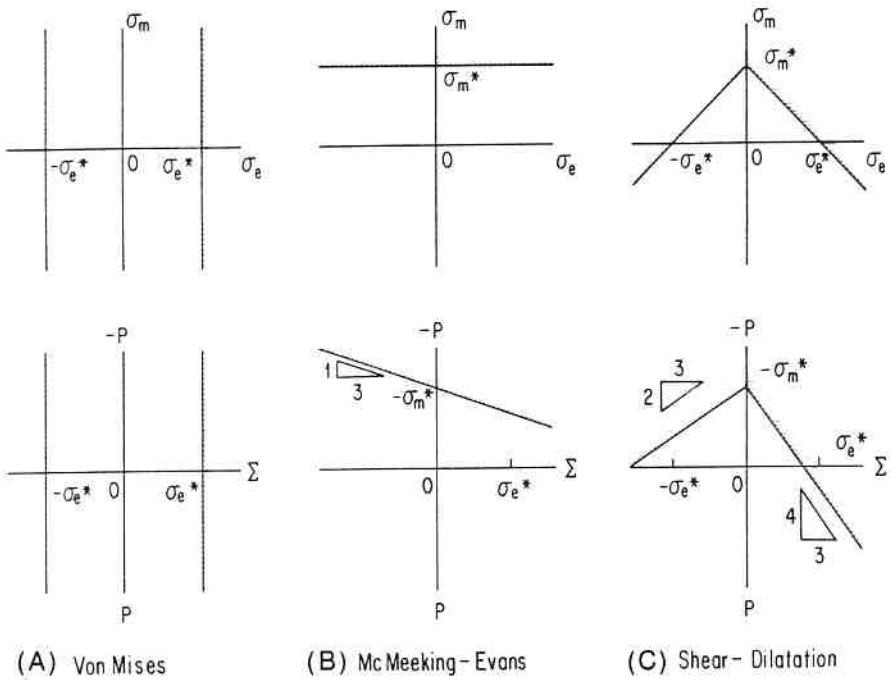

Fig. 7. Yield loci based on (*A*) shear only, (*B*) dilatation only, and (*C*) combined yield criteria.

ening, as evidenced by the substantial rise of the flow stress with increasing fraction of transformation, is noted. This is due to the potency distribution of nucleating sites[5,6] and the exhaustion of the transformable material element. Depending on the extent of transformation in a particular specimen, compressive flow stress between 1.0 and 1.8 GPa at zero pressure may be used for correlation.

The dependence of the macroscopic yield stress on the state of stress can be formulted as a yield criterion containing the two stress invariants. They are the equivalent stress

$$\sigma_e = \sqrt{3\sigma'_{ij}\sigma'_{ij}/2} \tag{5}$$

and the mean stress

$$\sigma_m = \delta_{ij}\sigma_{ij}/3 \tag{6}$$

In the above, the stress deviator is defined as before

$$\sigma'_{ij} = \sigma_{ij} - \delta_{ij}\sigma_{ij}/3 \tag{7}$$

The simplest yield criterion which is invariant is thus

$$\sigma_e/\sigma_e^* + \sigma_m/\sigma_m^* = 1 \tag{8}$$

in which σ_e^* and σ_m^* are the characteristic equivalent stress and the characteristic mean stress at which transformation plasticity ensues under a monotonic stress state. The actual stress components at the yield may increase or decrease from these characteristic values under a combined stress state. The form of the yield criterion was chosen because the coupling between the external stresses and the transformation strains, serving as the driving force assisting the transformation, is bilinear in stress and strain. Furthermore, the experimental data,[6] with a compressive mean stress, were found to be consistent with this yield criterion. Our intent here is to explore its implications, assuming the same yield criterion to be applicable under other stress states.

We now consider the following cases.

(A) Hydraulic Compression: Here $\sigma_m = -(P + |\Sigma|/3)$ and $\sigma_e = |\Sigma|$, where $|\Sigma|$ is the uniaxial compressive stress and P is the hydraulic pressure. Let the compressive yield stress Y^c be related to P by an equation consistent with Eq. (8)

$$Y^c = Y_0^c + \alpha^c P \tag{9}$$

where Y_0^c is the compressive yield stress at zero pressure and α^c is a constant. The superscript c denotes compression. The above form of yield criterion is a modification of the conventional shear-stress-based one with the addition of pressure hardening, given by the coefficient α^c. Data from Fig. 6 and elsewhere[6] provide detailed information on Y_0^c and α^c at various fractions of transformation.

It can be shown from Eqs. (8) and (9) that

$$\sigma_e^* = 3Y_0^c/(\alpha^c + 3) \tag{10}$$

and

$$\sigma_m^* = Y_0^c/\alpha^c \tag{11}$$

It is found that α^c approaches 2 except at very small strains and later at very large strains, while the value of Y_0^c varies from 1.0 to 1.8 GPa as the fraction of transformation increases from 0 to 1. Thus, at $\alpha^c = 2$

$$(\sigma_e^*/\sigma_m^*)_{\text{macroscopic}} = 6/5 \tag{12}$$

In this case, shear and dilatant yield stresses are nearly of the same magnitude, and normality is approximately satisfied, as seen from Eqs. (3) and (12).

(B) Uniaxial Tension: Here $\sigma_m = \Sigma/3$ and $\sigma_e = \Sigma$. From substitution, the uniaxial yield stress in tension is found to be

$$Y_0^t = 3Y_0^c/(2\alpha^c + 3) \tag{13}$$

Taking $\alpha_c = 2$ as before, the above relation predicts $Y_0^t = 3/7 Y_0^c$.

At initial yielding, $Y_0^c = 1.1$ GPa; hence, $Y_0^t = 0.47$ GPa. Measurement by Marshall of tensile yield stress of Mg-PSZ at small yielding is in good agreement with the above value.[12]

(C) Indentation: As will be shown in the companion paper,[7] the stress state under the indent is essentially that of hydraulic compression, with $|\Sigma| = (2\alpha + 1)Y_0^c$ and $P = 2Y_0^c$ when the misfit dilatancy is neglected. The experimentally measured hardness gives $H = 8.2Y_0^c$, which is in tolerable agreement with $|\Sigma| + P$ or $(2\alpha + 3)Y_0^c$, when Y_0^c is chosen at 50% of full transformation. It can be more accurately predicted by a detailed elastic-plastic analysis given elsewhere.[7]

(D) Bending: In small-scale pure bending, the tensile side is expected to yield at a considerably lower stress while the compressive side remains elastic, according to Eq. (13). This has been confirmed by Matsui.[13] Initial yield should occur at the outer fibers on the tensile side at exactly Y_0^t. Subsequent deformation, however, will cause a shift of the neutral axis toward the compressive

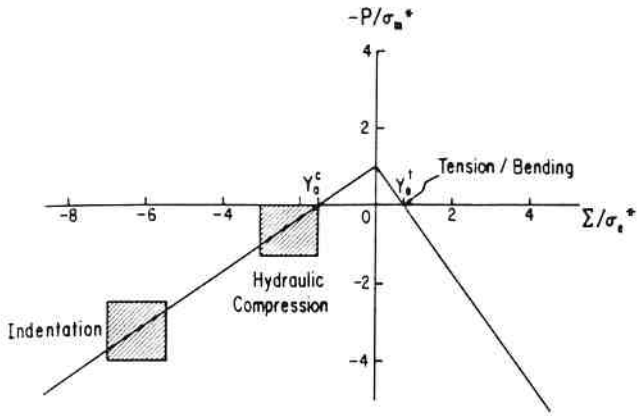

Fig. 8. Experimental regimes where the shear-dilatation yield criterion was verified. Stress state at tensile crack tip lies in first quadrant.

Table I. Experimental Observations of Shear and Dilatation Effects in Transformation Plasticity

Experiments	Material	Observation	Ref.
Indentation, fracture	Mg-PSZ, Ca-PSZ	Shear*	14, 15
Compression	Mg-PSZ, Y-PSZ	Shear	16
Bending	Y-TZP	Shear, polarity†	13
Tension, bending	Mg-PSZ	Polarity	12, 21
Indentation	Mg-PSZ	Pressure hardening‡	7

*Shear bands or shear variants along maximal shear stress direction. †Tensile yield much easier than compressive yield. ‡Yield stress enhanced by pressure.

side. Results obtained in the latter regime, such as bend strength, must be interpreted with this mechanical aspect in mind. The apparent bend strength is higher than the tensile strength for this reason.[12]

For comparison, we plot in Fig. 7 the yield loci in (σ_e, σ_m) and (Σ, P), and the corresponding yield loci in which only the shear (Von Mises criterion) or the dilatation (McMeeking-Evans criterion[12]) is considered. The regimes where the shear-dilatant yield criterion has received experimental confirmation are indicated in Fig. 8.

(4) Microscopic Stresses

When an external stress is applied, shape distortion of the transforming phase is aided by the external work which couples the external stress and the shape strain. Theoretically, the microscopic coupling between the applied stress and the shape strain depends on the orientation and the shear variant of the nucleus. If each shear band is triggered by a very small number of nuclei (say, one), it is reasonable to expect that the most favorably oriented crystallographic variant may be found in these nuclei, and the most favorable coupling should dominate the stress dependence. The microscopic coupling responsible in this case was found to be[5,6]

$$W_{max} = -P\bar{e}_T + \frac{|\Sigma|}{2}\left[s_T + \frac{\Sigma}{|\Sigma|}(\bar{e}_T + e_T)/2 + \left(\frac{\Sigma}{|\Sigma|} - \frac{1}{2}\right)(3e_T - \bar{e}_T)^2/4s_T\right] \quad (14)$$

where e_T is the normal transformation strain across the habit plane. On the other hand, if each shear band can only be triggered by a large number of nuclei, it is highly unlikely that *all* of these nuclei, which are as closely spaced as depicted in Fig. 3, do have the most favorably oriented variant in them. Rather, we expect that only some randomly oriented variants are available to most of these nuclei. If so, the microscopic coupling should be that of a randomly oriented variant. In that case[5,6]

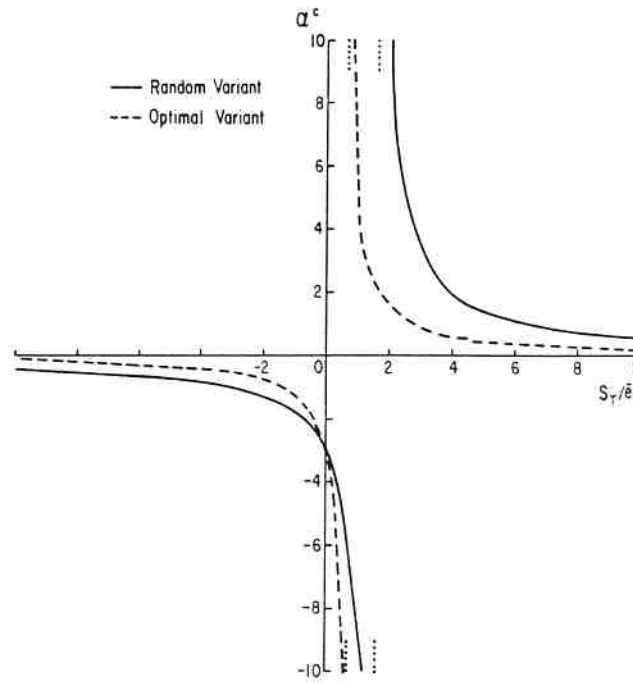

Fig. 9. Predicted pressure sensitivity in compression, as a function of shear and dilatation crystallographic strains.

$$W_{avg} = -P\bar{e}_T + \frac{|\Sigma|}{3}\left(2s_T/\pi + \frac{\Sigma}{|\Sigma|}\bar{e}_T\right) \quad (15)$$

The coefficient of pressure hardening can be calculated from Eqs. (14) and (15)

$$\alpha = (d|\Sigma|/dP)_w \quad (16)$$

From the above considerations, we expect the coefficient to be bounded by

$$\frac{2\bar{e}_T}{s_T + (\bar{e}_T + e_T)\Sigma/2|\Sigma|} \le \alpha \le \frac{3\bar{e}_T}{2s_T/\pi + \bar{e}_T\Sigma/|\Sigma|} \quad (17)$$

in which the lower bound derives from the maximum microscopic coupling and the upper bound derives from the average microscopic coupling. Results of α^c are plotted in Fig. 9 assuming $e_T = \frac{1}{3}\bar{e}_T$ for different ratios of $s_T/\bar{e}_T$. (Other values of e_T will only slightly alter the lower bound, but will not affect the upper bound.) For Mg-PSZ, $s_T/\bar{e}_T = 3.75$. The experimentally measured α^c is found to be very close to the upper bound. Thus, the microscopic coupling between the applied stress and the transformation strain is representative of a randomly oriented variant, which is consistent with the shear-band mechanism requiring a larger number of correlated nucleation events.

To assess the contribution of the shear and dilatation stresses more directly, we write

$$W = (|\Sigma|/\alpha - P)\bar{e}_T \quad (18)$$

which is equivalent to Eqs. (14) and (15) when the appropriate value of α is substitued into those expressions. Since $\alpha^c \approx 2$ in hydraulic compression, and $|\Sigma|/2$ is exactly the Tresca shear stress, it is concluded that the shear and dilatation components are roughly of the same weight. Note that the macroscopic Eq. (12) and the microscopic Eq. (18) are identical once proper correspondence is made between $(|\Sigma|, P)$ and (σ_s, σ_m).

In addition to our hydraulic compression experiments, other experimental observations of stresses and strains which bear on the shear and dilatation effects in zirconia-containing ceramics are summarized for future reference in Table I.

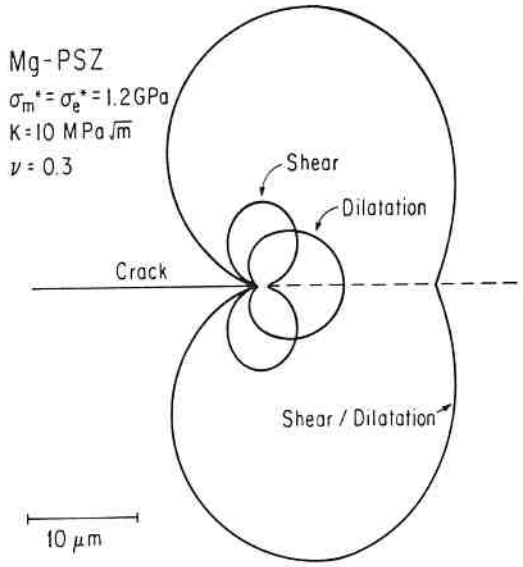

Fig. 10. Crack-tip process zone predicted by three yield criteria. Marker (10 μm) is scaled for Mg-PSZ of high toughness.

Table II. Radii of Transformation Zones Along and Perpendicular to Crack Extension Plane

θ	r_e (μm)	r_m (μm)	r (μm)
$\theta = 0$	1.76	8.30	17.8
$\theta = \pi/2$	9.17	4.15	25.7

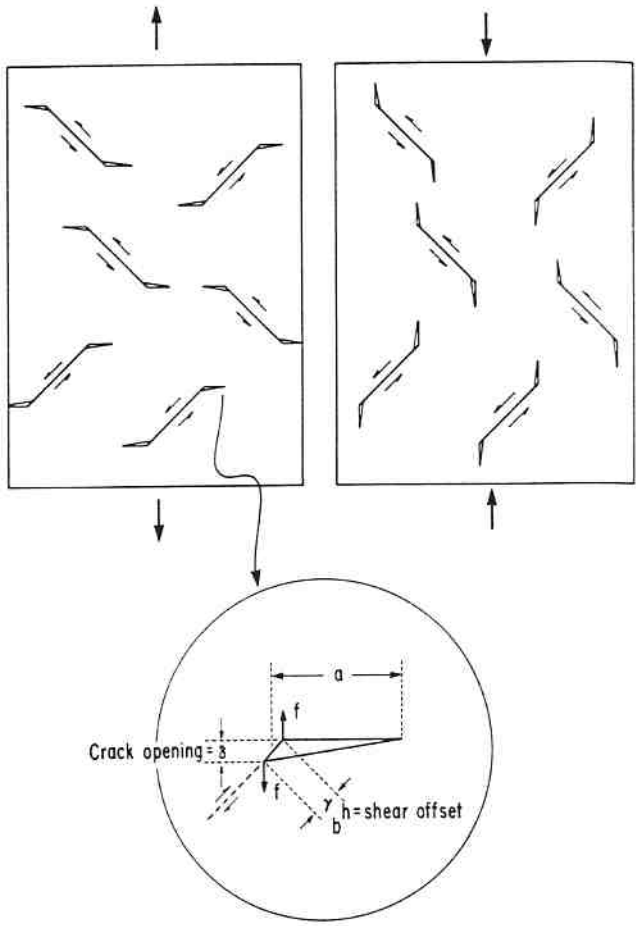

Fig. 11. Schematic mechanism of microcracking due to grain-boundary decohesion at intersections with shear bands. Note anisotropic orientation of microcracks.

IV. Shear and Dilatation Effects on Fracture

To assess the importance of the shear and dilatation effects on fracture of transformation-toughened ceramics, it is necessary to (a) examine the macroscopic process zone within which transformation takes place, providing crack-tip shielding and transformation toughening, and (b) examine the microstructures, containing microcracks and secondary damage, in the process zone in the wake of transformation plasticity. We now deal with these aspects separately.

(1) Crack-Tip Transformation Zone

At the tip of a stationary plane-strain crack loaded by a distant mode I stress intensity factor K, the unperturbed elastic solution for the principal stresses is

$$\begin{Bmatrix} \sigma_{\mathrm{I}} \\ \sigma_{\mathrm{II}} \\ \sigma_{\mathrm{III}} \end{Bmatrix} = \frac{K}{\sqrt{2\pi r}} \cos\frac{\theta}{2} \begin{Bmatrix} 1 - \sin\dfrac{\theta}{2} \\ 1 + \sin\dfrac{\theta}{2} \\ 2\nu \end{Bmatrix} \tag{19}$$

where θ is the angle from the crack extension plane and r is the radial distance from the crack tip. In the plane-stress condition, σ_{III} should vanish while other components remain the same.

Referring to the yield criterion of transformation plasticity, Eq. (8), we find it convenient to examine the condition of

$$\sigma_e = \sigma_e^* \tag{20}$$

and

$$\sigma_m = \sigma_m^* \tag{21}$$

respectively. At a radius r_e

$$r_e = \frac{1}{2\pi}\left(\frac{K}{\sigma_e^*}\right)^2 \cos^2\frac{\theta}{2}\left[(1 - 2\nu)^2 + 3\sin^2\frac{\theta}{2}\right] \tag{22}$$

the condition of Eq. (20) is met. Similarly, at a radius r_m

$$r_m = \frac{1}{2\pi}\left(\frac{K}{\sigma_m^*}\right)^2 \cos^2\frac{\theta}{2}\frac{4(1+\nu)^2}{9} \tag{23}$$

condition (21) is met. Finally, by substitution, it is found that the yield criterion, Eq. (8), is met within a radius r

$$r^{1/2} = r_e^{1/2} + r_m^{1/2} \tag{24}$$

or

$$r = \frac{K^2}{2\pi}\cos^2\frac{\theta}{2}\left\{\left[\sqrt{(1-2\nu)^2 + 3\sin^2\frac{\theta}{2}}\Big/\sigma_e^*\right] + \left[\frac{2}{3}(1+\nu)/\sigma_m^*\right]\right\}^2 \tag{25}$$

Similar solutions in the plane-stress condition are obtained by letting $\nu = 0$.

It is interesting to note that r_e is exactly the conventional radius of the plastic zone in fracture mechanics if σ_e^* is identified as the uniaxial yield stress. Likewise, r_m is exactly the radius of the transformation zone in the model of McMeeking and Evans[2] if σ_m^* is identified as their critical transformation stress. The above two radii correspond to the shear and dilatation criterion, respectively. The present yield criterion is more realistic, in that it is constructed from experiment and predicts a much larger transformation zone, according to Eq. (25).

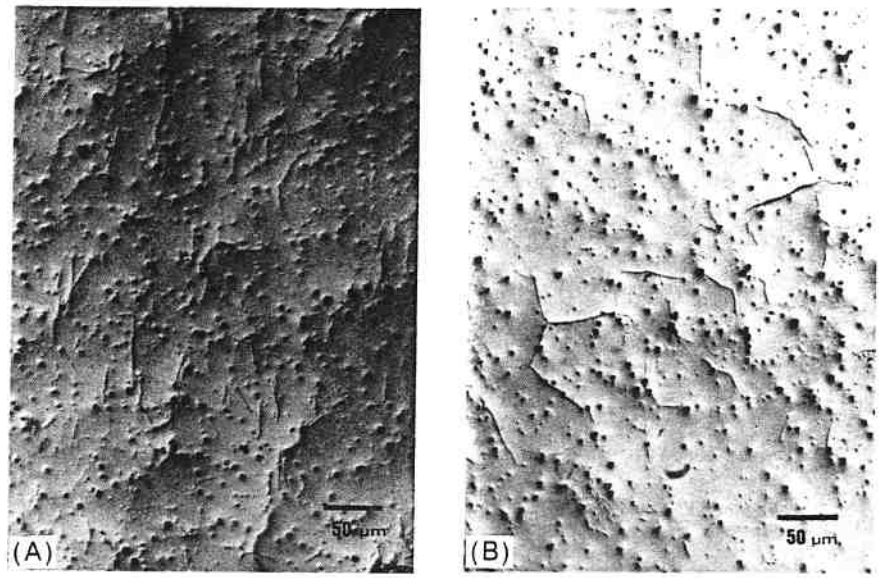

Fig. 12. (*A*) Longitudinal section of sample deformed nearly 100% under hydraulic compression; microcracks are axially oriented (vertical direction). (*B*) Transverse section showing microcracks along grain boundaries.

To appreciate the zone size and zone shape predicted from each of the above three criteria, we compute the radii r_e, r_m, and r at $\theta = 0$ and $\theta = \pi/2$ for $K = 10$ MPa·m$^{1/2}$. Values chosen for σ_s^* and σ_m^*, according to Eqs. (10) and (11) are both 1.2 GPa using $Y_0^c = 1.8$ GPa and $\alpha^c = 1.5$ at 100% or full transformation. (The value of α^c chosen here is slightly lower because the pressure-dependent transformation strain is nearly exhausted near full transformation.) These values are tabulated in Table II for $\nu = 0.3$ in the plane-strain condition. It can be seen that r_e and r_m are much smaller than r, indicating the very important combined effect of both the shear and the dilatation criteria. Overall, the two components are again of comparable weight in the forward zone of the crack tip. The zones are plotted in Fig. 10; we note that the computed value of r is within a factor or 2 of the experimentally observed zone size in Mg-PSZ at comparable toughness.[15,17]

Note that the actual value of r will vary somewhat if different α^c and Y_0^c are chosen. These properties are material dependent. In addition, if the yield criterion, unlike what is shown in Figs. 7 and 8, is somewhat curved, then the value of α^c is less certain and the extrapolation into the primarily tensile regime near the crack tip may not be very accurate. In view of these uncertainties, the tolerable agreement found here is very encouraging.

We also note that our prediction is based on ab initio calculations using experimental data on transformation plasticity. Previous models were not able to predict the zone size for lack of experimental information on σ_e^* and σ_m^*.[2-4]

Although the attendant toughening, ΔK, must scale with r, by a dimensional argument, the prediction of fracture toughness from crack-tip transformation plasticity at the steady state is not yet possible. Experimentally and theoretically, it was found[6] that the associated flow rule which would have simplified the relationship between the incremental strain and the current stress state does not always hold in transformation plasticity. Since a material element in front of the crack tip will experience nonproportional loading and unloading as the crack propagates, the residual stresses and strains of the material element, in the process zone and in the wake of the extending crack, are very complicated and must be computed numerically. Much more extensive knowledge of transformation plasticity during nonproportional loading and unloading is needed before such a computational task can be undertaken. In view of these complications and of the generally substantial contributions of the shear and dilatation stresses and strains to transformation plasticity, we tentatively conclude that the previously proposed models of transformation toughness need much further refinement[2-4] and the sometimes-claimed agreement between the measured toughness values and these models remains to be verified.[18]

Despite the above reservations, a decreasing σ_e^* or σ_m^* will definitely increase the process-zone size. As noted earlier, the increment of fracture toughness, ΔK, probably scales with r according to $\Delta K \propto r^{1/2}$, from a dimensional argument. In this respect, Eq. (24) strongly suggests that the toughness enhancements due to shear and dilatancy are to some extent additive. A toughness increment might be intuitively expected to result from crack-tip plasticity because the stress concentration is suppressed by yielding and the energy dissipation increased by plastic work. The linear form of the macroscopic criterion of yield stress, Eq. (8), and its microscopic counterpart of plastic work, Eqs. (14) and (15), seem to lend support to the above expectations.

(2) Microcracking

Where transformation plasticity proceeds in the process zone by shear localization, damage is accumulated at the same time by the intersection of shear bands and grain boundaries, leaving microcracks. While this type of damage has long been suspected, characterizing it at the crack tip is difficult, because of the poor statistics and the large closure forces therein. However, damage in a uniformly deformed specimen, as with hydraulic compression, has been recently studied in some detail, and a microscopic theory has been formulated.[19] The results of this study can shed light on damage in the process zone.

Microcracks in hydraulic compression are nucleated by the shear offsets between the shear bands and grain boundaries. That this is theoretically possible can be shown by a Zener-Stroh-type analysis[20,21] on the nucleation and growth of microcracks at shear band/grain boundary intersections, as will be reported elsewhere.[19] The microcracks are believed to be parallel to the loading direction, as schematically shown in Fig. 11 for compression damage. Micrographs taken from longitudinal and transverse sections, shown in Fig. 12, demonstrate the parallel distribution of microcracks in the former case and an essentially random distribution in the latter, as expected. These cracks are probably along the grain boundaries and are of the length of a grain, ca. 50 μm.

The anisotropic distribution of microcracks affects the elastic properties of the deformed material. Axial unloading measurements at the same pressure performed upon interruption of the hydraulic compression tests revealed that the unloading modulus along the axial direction suffers a smaller change, while the transverse Poisson's contraction is substantially reduced. These results are plotted in Fig. 13, in which data from two different tests are superimposed onto each other. Since the load-carrying capability along the axial direction is less affected by axial cracks than the transverse contraction, the elastic anisotropy manifested here is consistent with the microcracking mechanism depicted in Fig. 11.

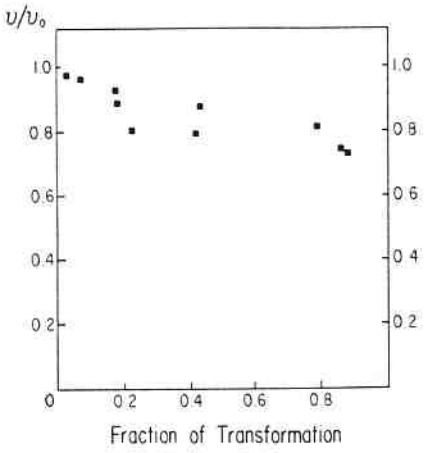

Fig. 13. Evolution of Poisson's ratio as a function of fraction of transformation. Data were obtained at pressures of 30 and 200 MPa under hydraulic compression.

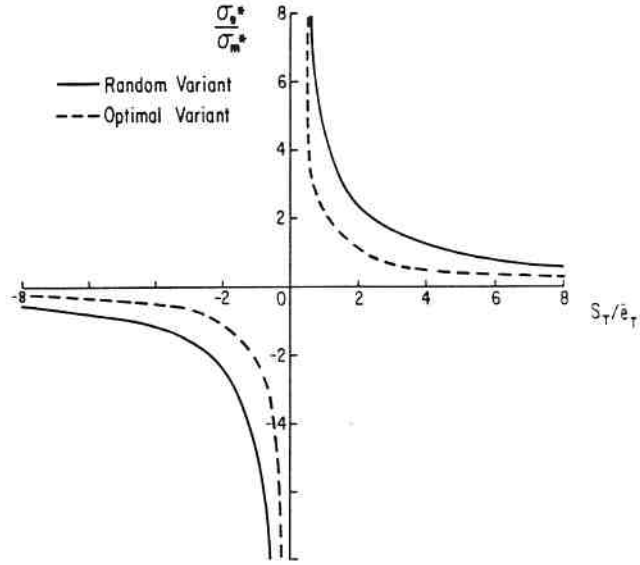

Fig. 14. Predicted ratio of shear and dilatation yield stresses as a function of shear and dilatation crystallographic strains.

As rationalized in Ref. 19, microcracks of the above type are the direct result of shear localization. Surprisingly, the damage that they incur seems to be independent of pressure and dependent only on the fraction of transformation (although pressure does indirectly reduce the tendency toward microcracking by delaying transformation). This apparent insensitivity to a direct pressure effect is probably due to the relatively low cohesion of ceramic grain boundaries, which tend to fracture to completion when intercepted by many parallel shear bands.[19] In other words, both nucleation and growth of grain-boundary microcracks are fairly easy in the presence of shear offsets.

Microcracks also contribute to an apparent dilatant strain in the normal direction. Since microcracking is anisotropic and strongly stress dependent, dilatancy due to microcracking is also anisotropic and stress dependent. The existence of the extra component of plastic strain of this origin further complicates the flow rule of transformation plasticity and the task of crack-tip modeling.

Thus, microcracking is primarily the result of the shear component of transformation plasticity, although its onset is indirectly affected by the dilatation component due to pressure hardening. In addition to causing material degradation, it acts directly as a dilatation mechanism. The highly anisotropic orientation of microcracks can be strongly influenced by the stress state.

V. Failure Control of Transformation-Toughened Ceramics

The understanding of transformation plasticity and fracture process zone from the previous sections enables us to take a broader perspective on the strategy of failure control of the ultimate transformation-toughened ceramics. While transformation-toughened ceramics of the earlier generation have a process zone as small as 0.5 μm and an unattractive toughness overall, several new alloys have a process zone 10 to 100 times larger. The implication of the impressive order-of-magnitude increase in process zone size is that some ultimate advanced ceramics may become tolerant of processing flaws in structural applications. In particular, at a reasonable tensile strength of 500 MPa, an ultimate transformation-ceramic with a fracture toughness of 20 MPa$\cdot$m$^{1/2}$ will be tolerant of a preexisting surface mode I flaw as long as 500 μm. It is reasonable to expect that processing flaws in excess of this size can be eliminated. Hence, the ultimate advanced ceramics will not be strength limited by preexisting flaws.

Our study of microcracking incurred by transformation plasticity, however, points to the other strength-limiting process in transformation-toughened ceramics. Near full transformation, a decrease in load-carrying area by as much as 30% may result from microcracks aligned perpendicular to the maximal principal stress direction, as suggested by the data on elastic properties given in Fig. 13. Microcracks of the length of a grain are responsible for this degradation. Such a high density of microcracks is clearly detrimental. Indeed, specimens failed even in hydraulic compression at this stage. In tension and bending, the available data have consistently showed that failure ensues shortly after initial yield at very small plastic strains, of the order of 10^{-3},[12,22,23] as recently noted by Swain.[24] Thus, in contrast to the case of metallic materials, the considerable strain-hardening capability of transformation toughening in ceramics cannot delay postyield failure effectively, because of the prevalence of microcrack damage. Nevertheless, the prospect of yield-limited strength, as opposed to flaw-limited strength, for transformation-toughened ceramics implies a significant simplification of design philosophy and improvement of product reliability. The undesirable strength distribution of Weibull statistics resulting from residual flaws can in principle be removed from engineering consideration. These advantages cannot be overemphasized in many advanced structural applications.

We thus foresee exciting future exploitation of transformation-toughened ceramics which are flaw tolerant and yield limited. For optimal applications, special attention must be paid to the unique stress-state sensitivity of the yield stress of transformation plasticity. The degree of stress-state sensitivity depends on the relative importance of shear and dilatation in transformation plasticity and is best signified by the coefficient of pressure hardening. It might reasonably be expected that most alloys will follow the random-variant prediction of pressure sensitivity depicted in Fig. 9, which is replotted in terms of σ_e^*/σ_m^* using Eqs. (10) and (11) in Fig. 14. In zirconia-containing ceramics, we expect α^c to lie near or slightly below 2, in view of the ratio of shear and dilatation in the *t-m* transformation. The corresponding ratio of σ_e^*/σ_m^* is 1.2, while the ratio of compressive yield and tensile yield is $\frac{2}{3}$ (see Section III). Evaluations of other potential candidate systems for transformation toughening may also proceed along this line of reasoning.

References

[1]R. C. Garvie, R. H. Hannink, and R. T. Pascoe, "Ceramic Steel," *Nature (London)*, **258** [5537] 703–704 (1975).

[2]R. McMeeking and A. G. Evans, "Mechanisms of Transformation Toughening in Brittle Materials," *J. Am. Ceram. Soc.*, **65** [5] 242–45 (1982).

[3]B. Budiansky, J. W. Hutchinson, and J. C. Lambropoulos, "Continuum Theory of Dilatant Transformation Toughening in Ceramics," *Int. J. Solids Struct.*, **19** [4] 337–55 (1983).

[4]J. C. Lambropoulos, "Shear, Shape and Orientation Effects in Transformation Toughening," Rept. MECH–55, Harvard University, Cambridge, MA, 1984.

[5]I-W. Chen, "Mechanisms of Transformation and Transformation Plasticity in ZrO_2-Containing Ceramics"; pp. 55–79 in Zirconia Ceramics, Vol. 4. Edited by S. Somiya and M. Yoshimura. Tokyo Institute of Technology, Yokohama, Japan, 1984.
[6]I-W. Chen and P. E. Reyes Morel, "Theory and Experiment of Transformation Plasticity in Brittle Ceramics. I. Yield Criterion and Flow Rule"; to be published in *Acta Metall.*
[7]I-W. Chen, "Implications of Transformation Plasticity in ZrO_2-Containing Ceramics: II. Elastic-Plastic Indentation"; this issue, following article.
[8]I-W. Chen and Y-H. Chiao, "Martensitic Nucleation in ZrO_2," *Acta Metall.*, **31** [10] 1627–38 (1983).
[9]I-W. Chen and Y-H. Chiao, "Martensitic Transformation in ZrO_2 and HfO_2 — An Assessment of Small-Particle Experiments with Metal and Ceramic Matrices"; pp. 33–45 in Advances in Ceramics, Vol. 12, Science and Technology of Zirconia II. Edited by N. Claussen, M. Rühle, and A. H. Heuer. American Ceramic Society, Columbus, OH, 1984.
[10]I-W. Chen and Y-H. Chiao, "Theory and Experiment of Martensitic Nucleation in ZrO_2-Containing Ceramics and Ferrous Alloys," *Acta Metall.*, **33** [10] 1827–45 (1985).
[11]I-W. Chen, Y-H. Chiao, and K. Tsuzaki, "Statistics of Martensitic Nucleation," *Acta Metall.*, **33** [10] 1847–59 (1985).
[12]D. B. Marshall, "Strength Characteristics of Transformation-Toughened Zirconia"; this issue, pp. 173–80.
[13]M. Matsui, "Transformation Plasticity in Y-TZP"; this issue, pp. 198–202.
[14]R. H. J. Hannink and M. V. Swain, "A Mode of Deformation in Partially Stabilized Zirconia," *J. Mater. Sci.*, **16** [5] 1428–30 (1981).
[15]M. V. Swain and R. H. J. Hannink, "*R*-Curve Behavior in Zirconia Ceramics"; pp. 225–39 in Advances in Ceramics, Vol. 12, Science and Technology of Zirconia II. Edited by N. Claussen, M. Rühle, and A. H. Heuer. American Ceramic Society, Columbus, OH, 1984.
[16]J. Lankford, "Plastic Deformation of Partially Stabilized Zirconia," *J. Am. Ceram. Soc.*, **66** [11] C-212–C-213 (1983); and private communication.
[17]D. R. Clarke; private communication.
[18]R. M. Cannon and A.G. Evans; to be published.
[19]I-Wei Chen, P. E. Reyes Morel, and G. Rodin, "Theory and Experiment of Transformation Plasticity in Brittle Solids. II. Microcracking and Fracture"; to be published.
[20]C. Zener; p. 3 in Fracture of Metals. American Society for Metals, Metals Park, OH, 1948.
[21]A. N. Stroh, "A Theory of the Fracture of Metals," *Adv. Phys.*, **6**, 418–65 (1957).
[22]K. Tsukuma and M. Shimada, "Strength, Fracture Toughness and Vickers Hardness of CeO_2-Stabilized Tetragonal ZrO_2 Polycrystals (Ce-TZP)," *J. Mater. Sci.*, **20** [4] 1178–84 (1985).
[23]D. C. Larsen and J. W. Adams, Rept. IITRI–MO 6117-15. Illinois Institute of Technology Research Institute, Chicago, IL, 1984.
[24]M. V. Swain, "Limitation of Maximum Strength of Zirconia-Toughened Ceramics by Transformation Toughening Increment," *J. Am. Ceram. Soc.*, **68** [4] C-97–C-99 (1985). □

J. Am. Ceram. Soc., **69** [3] 189–94 (1986)

Implications of Transformation Plasticity in ZrO_2-Containing Ceramics: II, Elastic-Plastic Indentation

I-WEI CHEN*

Department of Nuclear Engineering and Department of Materials Science and Engineering, Massachusetts Institute of Technology, Cambridge, Massachusetts 02139

Indentation hardness of partially stabilized zirconia was found to be 8.2 times the uniaxial compressive yield stress. This ratio is anomalously high for ceramic materials and is attributed to pressure hardening in transformation plasticity. An analytic solution of elastic-plastic indentation using the spherical-hole model is given, based on a pressure-sensitive idealized yield criterion. The theory correctly predicts a higher hardness and a larger plastic zone, both in quantitative agreement with the experimental observations in Mg-PSZ. Data analysis further reveals a large disparity of yield stress and hardness values among cubic, tetragonal, and monoclinic zirconias, resulting from their different phase transformation and twinning capabilities. The broader implications of pressure sensitivity in elastic-plastic indentation are rationalized.

Received July 12, 1985; revised copy received November 20, 1985; approved December 5, 1985.
Supported by the U.S. Department of Energy under Grant No. DE-FG 02–84ER45154.
*Member, the American Ceramic Society.

I. Introduction

IN ENGINEERING applications, microindentation is widely used for materials characterization, especially in the ceramic field. In view of its importance, an elastic-plastic analysis of indentation response which takes special notice of the salient features of transformation plasticity is clearly desirable. On the other hand, the very nature of indentation plasticity, which has a more complicated and rather unique stress state, affords in turn an interesting opportunity to further examine the implication of transformation plasticity in zirconia-containing ceramics, as outlined in the companion paper.[1] In particular, potentially prominent pressure-sensitive effects on microindentation can be explored. In this regard, a quantitative analysis of indentation plasticity not only sheds light on the indentation phenomena, but presents itself as a severe test of the constitutive equation of transformation plasticity formulated therein.[1] The purpose of the present study is to provide such an analysis and assessment.

While the phenomena in transformation plasticity are unusually rich, e.g., pressure sensitivity, strain hardening, strain localization, nonnormality, and microcracking,[1–3] we shall nevertheless conduct our analysis of indentation mostly with a simplified consti-